STUDIA UBB CHEMIA, LXX, 4, 2025 (p. 23-39)
(RECOMMENDED CITATION)
DOI:10.24193/subbchem.2025.4.02

ELECTROCHEMICAL pH-STAT AS ACIDITY MONITORING SYSTEM IN HIGH IONIC STRENGTH SOLUTIONS. I. DESIGN CHALLENGES AND PRELIMINARY RESULTS

Gabriele-Mario BOGDAN[a], Sorin-Aurel DORNEANU[b,*]

ABSTRACT. Quantifying acidity has evolved from early attempts in the 1300s to the modern glass electrode pH sensor, which is difficult to implement for monitoring acid concentration in highly saline solutions. In this study a membrane-based filter-press electrochemical reactor functioning as a pH-stat that correlates current with acid concentration was tested. The behavior of HBr in KBr solutions was characterized, after which spectroscopic measurements of Alizarin Red S provided calibration curves used to validate glass electrode data. Reactor design principles and challenges were discussed, after which its behavior under non-polarized and polarized conditions was studied, concluding with two pH-stat tests, where different HBr concentrations were simulated by changing the acid molar flow rate, with pH values corroborated by spectroscopic measurements. A linear relationship was demonstrated between steady state current and acid molar flow rate. Imperfect membranes resulted in systematic errors between the amount of acid introduced and that neutralized. Preliminary results confirmed the feasibility of the electrochemical cell as an acid monitoring system, with future upgrades including PID control and design optimization.

Keywords: *glass electrode, pH-stat, electrochemical cell, acid concentration, high ionic strength*

INTRODUCTION

Quantifying the acidity of solutions has been attempted since at least the 1300s, when the first documented use of litmus was attributed to Arnaud de Villeneuve [1,2]. However, progress in understanding acidity was slow

[a] *Department of Chemical Engineering, Faculty of Chemistry and Chemical Engineering, Babeş-Bolyai University, 11 Arany Janos Street, RO-400028, Cluj-Napoca, Romania*
[b] *Interdisciplinary Research Institute on Bio Nano Sciences, Babeş-Bolyai University, 42 Treboniu Laurian Street, RO-400271, Cluj-Napoca, Romania*
[*] *Corresponding author: sorin.dorneanu@ubbcluj.ro*

until Arrhenius proposed the first modern acid-base theory, which was later refined by Brønsted and Lowry [3]. Defining acidity as a function of H^+ concentration led to the rapid development of detection and quantification methods and, eventually, to the invention of the glass electrode pH sensor, which is still widely used today [4]. A well-known limitation of glass electrodes is the so-called “sodium error”, where the sensor response becomes non-linear as it transitions from H^+ selectivity to Na^+ selectivity, phenomenon which also occurs, to a lesser extent, with K^+ [5,6]. In addition to the sodium error, Debye, Hückel (and later improvements to their theory) demonstrated that, in real solutions, ion-ion and ion-solvent interactions result in modified activity of solution components [6–9]. As a result, complex corrections based on activity coefficient models such as extended Debye-Hückel [7] and the Pitzer equations [10] must be implemented, both of which require precise information about solution composition and physical properties to provide accurate predictions. All these factors make the implementation of the classic glass electrode as H^+ concentration monitoring system very difficult or even impractical, especially in high ionic strength solutions.

Alternatively, another common method for monitoring H^+ concentration is acid-base titration using either chemical or electrochemical methods [11–14], with the main advantage of enabling precise composition monitoring through stoichiometry. One such apparatus is the classic pH-stat, which combines data from a pH sensor with an automated acid/base injection system to maintain pH at a constant value [15]. Various assembly variants and control schemes have been proposed in the almost one hundred years since its invention [11,12,16–19], but the topic receives increased attention especially in the biology modern literature. The aim of this paper is to design and test an ion exchange membrane (IEM) based filter-press electrochemical reactor (FPER) as pH-stat able to function as an acid concentration analyzer for a HBr/KOH electrosynthesis process. Our previous studies have demonstrated the possibility of using a four-compartment FPER for the electrosynthesis of KOH and HBr, with applications in a base metals recycling process from waste printed circuit boards (WPCBs) [20]. Preliminary process monitoring results have shown H^+ activities up to 20 times higher than expected for HBr in 2 M KBr solutions at most concentrations. In this work the discrepancy between H^+ concentration and measured pH was addressed and a more accurate and reliable real-time acidity monitoring system using a membrane-based electrochemical pH-stat was developed. To achieve this, first, the pH evolution was studied in HBr solutions of concentrations between $5 \cdot 10^{-5}$ M and $5 \cdot 10^{-1}$ M in KBr of $2 \cdot 10^{-3}$, $2 \cdot 10^{-2}$, $2 \cdot 10^{-1}$ and 2 M. Next, spectroscopic data for Alizarin Red S (ARS) was acquired, enabling the correlation between its absorption spectra at 522 and 422 nm with pH, which will serve to validate the glass

electrode data during pH-stat experiments. Finally, the FPER was tested, and its passive and active behavior determined. Increasing HBr concentrations were simulated by varying the molar flow rate of HBr, and its performance as an acidity monitoring system was evaluated.

RESULTS AND DISCUSSION

pH measurements in KBr solutions

Senanayake [21] proved the complex behavior of proton activity in HCl + $CaCl_2$ and highlighted the numerous factors (ion hydration number, liquid junction potential between the test solution and the reference solution inside the sensor, etc.) necessary to establish a reliable correlation between pH and real acid concentration.

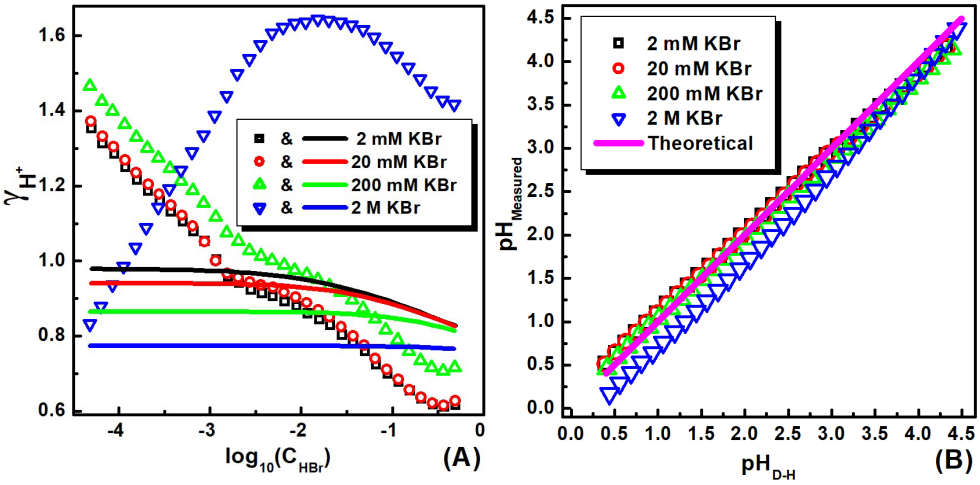

Figure 1. Correlation between the proton activity factor (γ_{H+}) calculated by D-H (line) and from measured pH values (symbols) and log(C_{HBr}) (A) and measured pH and computed pH using the D-H theory (B) for different concentrations of KBr indicated in inserts.

To determine the effect of these interactions in the HBr/KBr system, solutions of varying HBr and KBr concentrations were prepared to be used in controlled addition tests. Base solutions of $2 \cdot 10^{-3}$, $2 \cdot 10^{-2}$, $2 \cdot 10^{-1}$ and 2 M KBr with 10^{-5} M HBr were prepared, while the addition solutions had the same

concentrations of KBr with 1 M HBr. For the effective addition tests, 25 mL of base solution were introduced in a mixing cell using a calibrated pipette, over which 25 mL of addition solution was introduced in pre-calculated volumes using a calibrated peristaltic pump, resulting in constant KBr concentration and HBr concentrations ranging from $5 \cdot 10^{-5}$ M to $5 \cdot 10^{-1}$ M. Real activity coefficients were calculated by dividing the proton activity obtained from measured pH and real H^+ concentration and compared in Figure 1.A with the theoretical ones obtained with Debye-Hückel (D-H) theory. Furthermore, theoretical activity coefficients were used to compute theoretical pH values, which were plotted against the measured pH values, presented in Figure 1.B.

The results presented in Figure 1.A indicate that KBr concentration significantly impacts proton activity, especially at high concentrations. Interestingly, the calculated activity coefficients for HBr concentrations between $5 \cdot 10^{-5}$ and $5 \cdot 10^{-3}$ exceed unity in the lowest ionic strength solutions, in direct contradiction with D-H. This strange behavior at low H^+ concentrations can be attributed to CO_2 absorbed from the atmosphere, though its effect is negligible at higher HBr concentrations.

Additionally, it is evident that the D-H theory is insufficient to properly account for variations in the proton's activity factor. While D-H provides reasonable correction at 2, 20, and 200 mM KBr, even small pH errors translate into large concentration errors, especially in 2 M KBr. This confirms that, without proper and more complex corrections, glass electrodes are unsuitable for H^+ concentration monitoring under the required conditions.

Finally, the extremely large discrepancy between proton activity and concentration observed in our previous study could not be replicated, suggesting that the initial discrepancy observed may have been caused by a compromised pH electrode.

Spectroscopic measurements of Alizarin Red S

To validate the pH measurements obtained from our pH sensor, ARS was used as a reference pH indicator due to its three distinct colors: yellow, red, and purple in acidic (pH < 6.3), neutral and highly basic (pH > 9.4) solutions, respectively. Preliminary spectroscopic measurements were taken by controlled neutralization of HBr + 2 M KBr solutions with varying acid concentrations using KOH to obtain calibration curves. Example spectra for ARS under different pH conditions are presented in Figure 2.

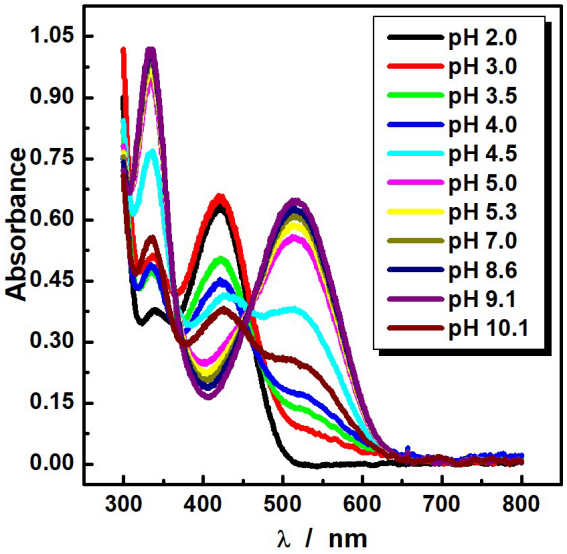

Figure 2. Examples of spectra obtained for ARS at different pH values during the neutralization tests.

The biggest absorption peaks can be observed around 422 nm under acidic conditions and 522 nm under basic conditions, with an inverse proportional relationship between the two. Inagawa et al. [22] proposed a relationship between pH and absorbance for indicators:

$$\log \frac{A(\lambda)-A_{In,\infty}}{A_{HIn,\infty}-A(\lambda)} = -pH + pK_a \quad (1)$$

where $A_{In,\infty}$ and $A_{HIn,\infty}$ represents the absorption of the indicator at the specific wavelengths in the protonated and deprotonated species, whereas A(λ) represents the absorbance at a given wavelength. In the case of ARS, the specific wavelengths for the protonated and deprotonated forms are approximately 422 and 522 nm, respectively, which are also the wavelengths we study. To eliminate errors resulting from the experimental setup, the ratio between the absorption at 522 and 422 nm, called $R_{522/422}$, was used instead of A(λ). In turn, the terms $A_{In,\infty}$ and $A_{HIn,\infty}$ become $R_{In,\infty}$ and $R_{HIn,\infty}$ and represent the ratio between the absorption in the deprotonated and protonated forms respectively, resulting in the following relationship:

$$pH = \log \frac{R_{HIn,\infty} - R_{522/422}}{R_{522/422} - R_{In,\infty}} + pK_a \quad (2)$$

The resulting ratios for the preliminary addition tests are presented in Figure 3. Optimal values for $R_{HIn,\infty}$ and $R_{In,\infty}$ and pKa were obtained by non-linear fitting using JMP 18 Student Edition software.

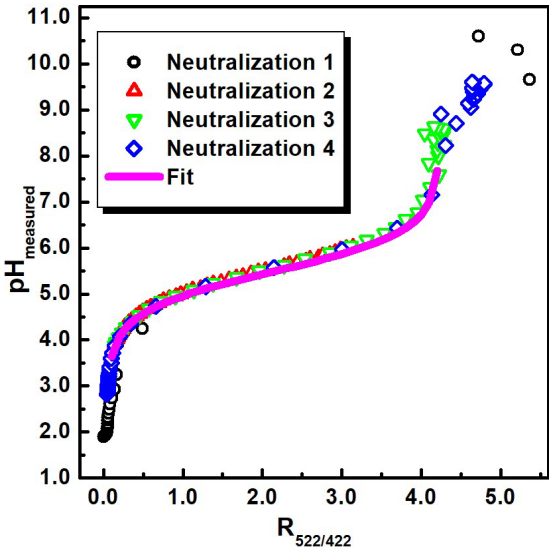

Figure 3. Preliminary calibration curves obtained through controlled neutralization and the resulting fit for ARS using equation (2).

The resulting pKa value from the fit was 5.48, which is in excellent agreement with literature data for similar spectroscopic measurements of ARS [23]. This confirms that, around pH 5, the response of the glass electrode is accurate, even in high ionic strength solutions.

As can be observed from Figure 3, $R_{HIn,\infty}$ and $R_{In,\infty}$ represent the left and right vertical asymptotes of the graph, where $R_{HIn,\infty}$ approaches 0 due to the complete absence of a peak at 522 nm in the protonated form, whereas $R_{In,\infty}$ is 4.2 due to the large baselines of the surrounding peaks which increase the absorption value at 422 nm. These neutralization tests demonstrate the possibility of correlating spectroscopic measurements with real pH values; thus, Alizarin Red S can be used as a pH reference to validate glass sensor measurements.

FPER passive behavior tests

In order to evaluate the passive FPER behavior (without polarization), four diffusion tests (see experimental section) were performed using 0.1 M and 1 M KOH as anolyte and catholyte, with results presented in Figure 4. The time lag between the first three diffusion tests using 1 M KOH can be attributed to slightly different starting pH values. Due to the fast neutralization process using 1 M KOH, the behavior of 0.1 M KOH was also evaluated, resulting in a much slower neutralization speed.

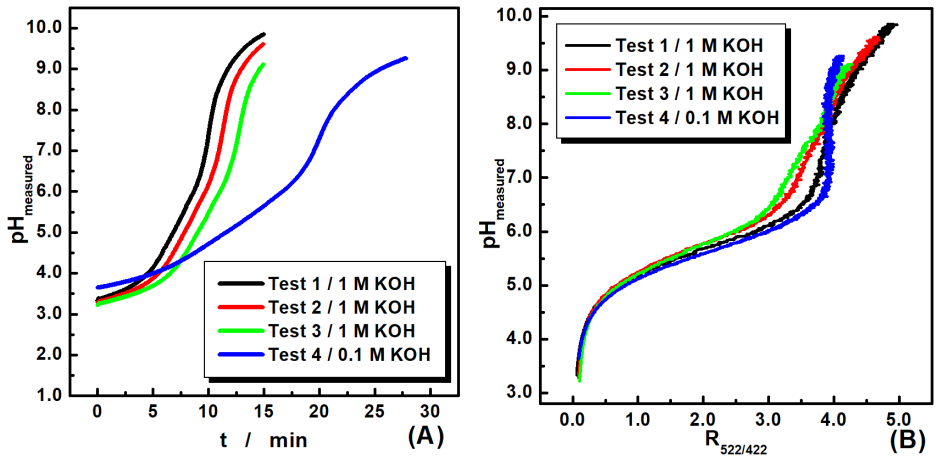

Figure 4. Results concerning the diffusion tests performed using 1 M and 0.1 M KOH as anolyte and catholyte: (A) evolution in time of measured pH; (B) the variation of measured pH in respect with the $R_{522/422}$ ratio.

For the first three diffusion tests the $pH_{measured}=f(R_{522/422})$ dependency does not follow the law described by Equation 2; however, the test using 0.1 M KOH fits very well. These unusual results obtained for the 1 M KOH diffusion tests can be attributed to insufficient mixing by the magnetic stirrer, which could not operate at high enough rotations per minute (RPM) due to risk of hitting the sensors. To solve this problem, a shielded electric motor designed for rotating disk electrodes was used, to which a stirring rod was attached using a brass collet. For precise control over mixing conditions, the electric motor was connected to a tachy-processor able to impose rotation speeds between 10 and 10000 RPM and was operated at 1000 RPM. Under the new mixing conditions, two diffusion tests were performed using 0.1 M KOH, and the results are presented in Figure 5. The resulting $pH = f(R_{522/422})$

correlation curves presented in Figure 5.B overlap perfectly, demonstrating the efficacy of the new mixing system and the reliability of ARS as a reference indicator.

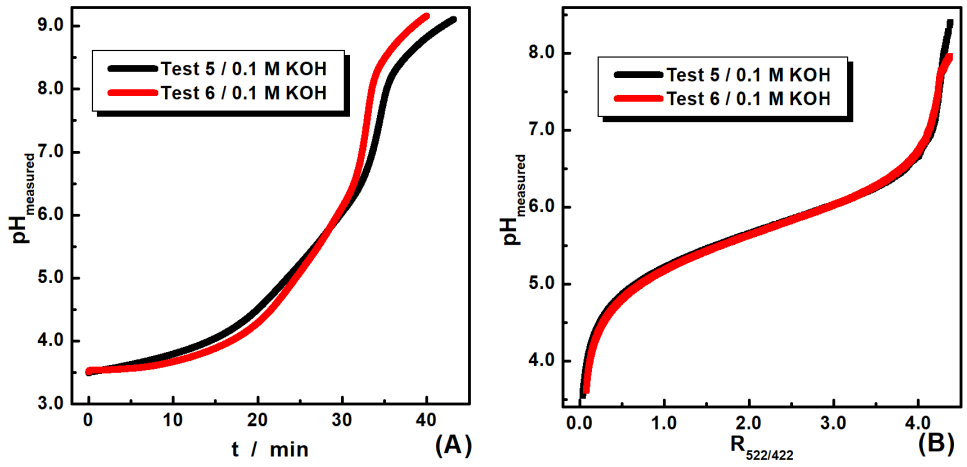

Figure 5. Results concerning the diffusion tests performed using 0.1 M KOH as anolyte and catholyte using the improved mixing system: (A) evolution in time of measured pH; (B) the variation of measured pH in respect with the $R_{522/422}$ ratio.

Effectively, the process that took place in the reactor during the diffusion tests is called Donnan dialysis, where, under the driving force of concentration gradients (and cross-membrane potentials arising from these gradients), ions migrate selectively through the IEMs [24,25]. Consequently, the neutralization speed observed is the result of two main parallel processes: (i) the diffusion of OH^- through the anion exchange membrane (AEM) and the subsequent neutralization of H^+, and (ii) the diffusion of H^+ through the cation exchange membrane (CEM) into the electrode compartment and its subsequent neutralization. To a lesser extent, since the membranes are not perfectly selective, a small quantity of H^+ diffused through the AEM into the cathodic compartment and, on the other side, a small quantity of OH^- diffused from the anodic compartment into the middle one. Additionally, K^+ and Br^- also migrated into the electrode compartments, thus contaminating the KOH fluxes with KBr. This is not an issue in our process due to specifics, however; different implementations must consider these ion diffusion effects when the reactor is idle.

The resulting correlation curves were fitted using Equation 2 in JMP 18 Student Edition for all diffusion tests performed using 0.1 M KOH and the resulting fitted coefficients are presented in Table 1.

Table 1. Fitted coefficients of equation (2) for preliminary controlled additions and all diffusion tests using KOH 0.1 M

Param.	Controlled Additions (Figure 3)	Test 4 0.1 M KOH	Test 5 0.1 M KOH	Test 6 0.1 M KOH	Average
pKa	5.483	5.635	5.707	5.725	5.638
$R_{HIn,\infty}$	0.039	0.050	0.008	0.045	0.036
$R_{In,\infty}$	4.227	4.158	4.382	4.38	4.287

For validation of pH measurements, the averages of all fitted coefficients will be used. The average pKa value is also within the reported pKa range for ARS in literature [23].

Manual pH-stat experiments

After the passive behavior of the FPER was determined, the next step was to observe its behavior under operational conditions. To do this, 50 mL of 0.5 M HBr + 2 M KBr solution dyed with 1 mL of 0.0125 M ARS was prepared, which results in the same ARS concentration as that in the FPER. Fresh solutions of 1 M KOH were prepared and introduced in the buffer tanks of the electrode compartments after which the middle compartment and its liquid circuits were washed with distilled water then filled with the same solutions as described previously.

The first manual pH-stat experiment was conducted prior to identifying the mixing problem and it played a key role in debugging the experimental setup error. To start the experiment, the anodic compartment (AC) and the cathodic compartment (CC) were filled with the 1 M KOH solution from the buffer tanks. The electrodes were polarized, after which varying molar acid flow rates (N_{HBr}), meant to simulate increasing HBr concentration, were injected in the reactor. The current was manually adjusted until pH values remained relatively stable. The evolution of pH, current through the working electrode (I_{WE}) and N_{HBr} over the course of the experiment are presented in Figure 6. Additionally, glass electrode pH data was compared to pH values calculated from the measured $R_{522/422}$ ratio.

The HBr molar flow rate was adjusted 5 times in equal increments between 37.5 and 187.5 μmol/min of HBr. The pH and spectroscopic measurements during this pH-stat test are very noisy due to improper mixing of the solution, which is evident at higher molar flow rates; however, they are in good agreement with each other.

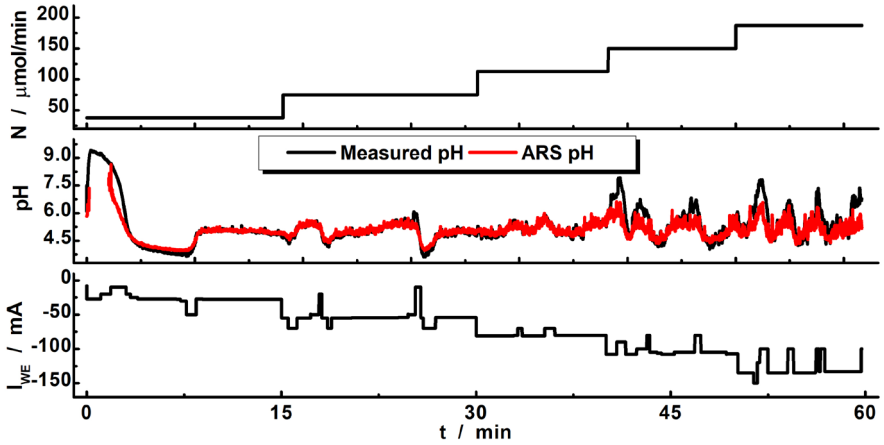

Figure 6. The evolution of N_{HBr}, measured and calculated pH from $R_{522/422}$ ratio, and current during the first manual pH-stat experiment.

After deploying the new and improved mixer, another manual pH-stat experiment was conducted. The FPER was set up in the same way as before, but the CC and AC were filled with 0.1 M KOH. Target pH was around 5, chosen due to the high sensitivity of the calibration curve in that area and faster response from the glass electrode compared to near-neutral solutions. Additionally, N_{HBr} was adjusted for times, in equal increments, between 7.5 and 30 μmol/min of HBr. The evolutions of N_{HBr}, pH and I_{WE} over the course of the experiment are presented in Figure 7.

Using the improved mixing system, resulting pH values from the glass electrode and spectroscopic data show excellent agreement, with a significant reduction in measurement noise. For all acid injection flow rates, pH consistently stabilized around 5.2, indicating that the imposed current was sufficient for the complete neutralization of the introduced acid. To measure the effectiveness of the electrochemical cell as an acid concentration monitoring system, steady state current (I_{SS}) values were extracted for all tested N_{HBr} values and are presented in Figure 8.A. Additionally, the real amount of HBr neutralized, $N_{HBr,neutralized}$, was calculated using Faraday's law and compared against the theoretical value in Figure 8.B.

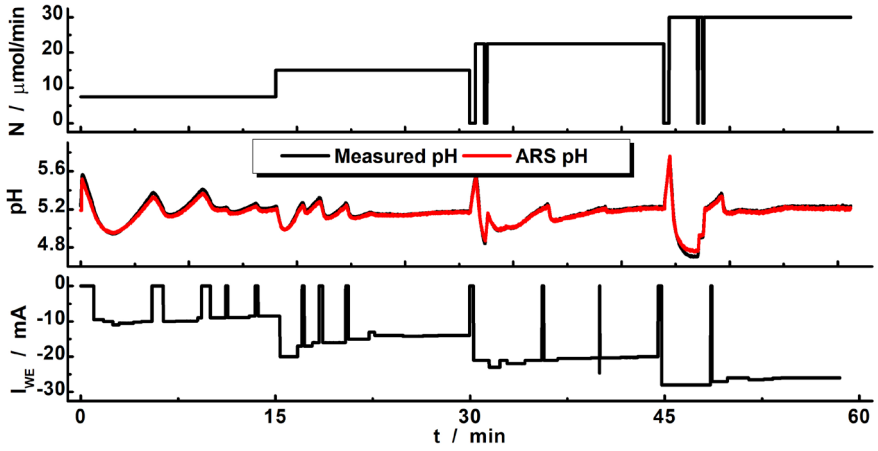

Figure 7. The evolution of N_{HBr}, measured and calculated pH from $R_{522/422}$ ratio, and current during the second manual pH-stat experiment.

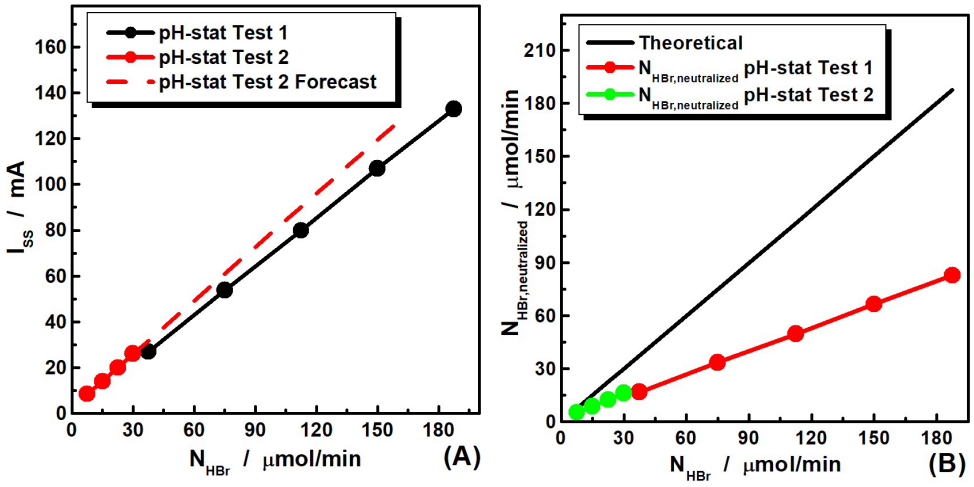

Figure 8. Influence of N_{HBr} on steady-state current during both manual pH-stat tests (A) and calculated neutralized molar fluxes using Faraday's law against theoretical values (B)

Figure 8.A shows that the relationship between N_{HBr} and I_{SS} is very linear ($R^2 > 0.999$) for both pH-stat tests, with a slight difference in slope. The difference in slope can be attributed to the faster diffusion of KOH through the IEMs at 1 M since, by extrapolating the data from the second pH-stat test, we can see that I_{SS} values are consistently lower than when

using 0.1 M KOH. Figure 8.B indicates that less acid than actually was neutralized, resulting in current efficiency over 100% for all N_{HBr} tested. This cannot be true, however, since for pH to remain constant, N_{HBr} and $N_{HBr,neutralized}$ must be equal. These conflicting results can be explained by the imperfect nature of the IEMs. In theory, under the influence of an electric field, the migration of ions towards the electrodes should account for the vast majority of mass transport through the membranes. However, Ozkul et al. [26] have shown that convection can represent up to 35% of the total ion flux through the membrane. Membrane charge density also plays a very important role in the ion selectivity of the membrane. Consequently, low charge density membranes induce significant membrane co-ion fluxes, negatively impacting ion selectivity [27,28]. The cumulative effect of these phenomena is constant, systematic and specific for a given system, meaning that it can be accounted for with periodic calibration of the FPER.

CONCLUSIONS

This study successfully elucidated the observed extremely large proton activity factor in the HBr + KBr system, simultaneously demonstrating the infeasibility of implementing glass electrode pH sensors as standalone H^+ concentration monitoring systems. Pertinent Alizarin Red S spectroscopic data was acquired, which enabled the obtaining of pH=f(R) correlation curves that served to validate glass electrode pH data. A filter-press electrochemical reactor using an anion exchange membrane and a cation exchange membrane was built and tested under passive and polarized conditions, which allowed for the identification and correction of design flaws. Two manual pH-stat tests were conducted by varying applied current for different acid injection flow rates, simulating real increase of HBr concentration during electrosynthesis, better results being obtained using the improved mixing system. FPER based pH-stat performance as an acidity monitoring system was evaluated, resulting in a very linear relationship between acid molar flow rate and steady state current. The discrepancy between the introduced acid molar flow rate and that neutralized calculated using Faraday's law was explained by imperfect membrane behavior. Further studies should focus on implementing PID (**P**roportional, **I**ntegral and **D**erivative) control of the system, acquiring more $I_{SS}=f(N_{HBr})$ data and optimizing the reactor design.

EXPERIMENTAL SETUP

Chemicals

All chemicals used were of analytical grade (p >99%). Solid KOH and KBr used in the preparation of all solutions containing these substances were purchased from Merck, Germany. HBr 48% from Merck, Germany was used for the preparation of stock HBr 2 M solution which was used for the preparation of all other solutions containing HBr. Standard buffer solutions HI 5007 of pH 7.01 and HI 5002 of pH 2.00 were purchased from Hanna Instruments, Romania and used for periodic calibration of the pH sensor. Alizarin Red S used for the preparation of stock 0.0125 M solution was also purchased from Merck, Germany. Double distilled water from a lab-grade distillation system was used for the preparation of all solutions in this study.

Filter press electrochemical reactor design

To neutralize the introduced acid, a three-compartment filter press electrochemical reactor equipped with an AEM, a CEM and two nickel electrodes was deployed. The electrochemical reaction taking place in the electrode compartments is water electrolysis in basic conditions. A detailed schematic of the reactor design is presented in Figure 9.

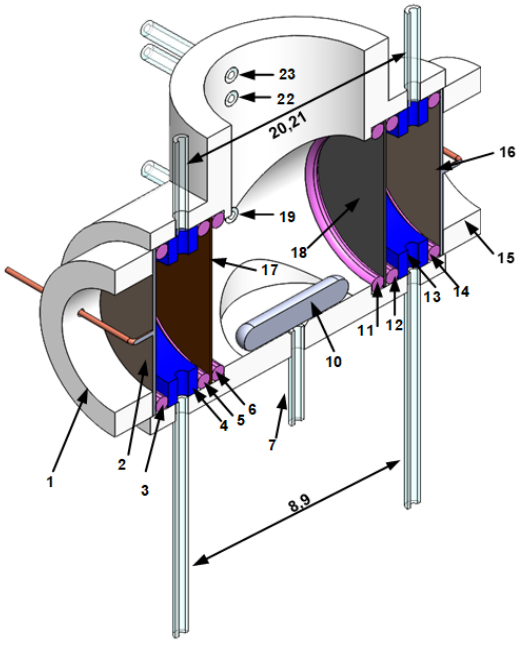

Figure 9. Detailed schematic of the initial FPER based pH-stat design. 1,15 – Pressing caps; 2,16 – Ni electrodes; 3,5,6,11,12,14 – Rubber O-rings; 4,13 – AC and CC spacers; 7 – Acid injection tube; 8,9 – AC and CC inlets; 10 – Magnetic stirrer; 17 - CEM; 18 – AEM; 19 – Z-cell inlet; 20-21 – AC and CC outlets; 22 – Overflow; 23 – Z-cell outlet

The reactor was assembled and pressed between two metal plates using screws. To ensure all the compartments are watertight, the screws were slowly tightened over the course of a few days to allow the O-rings to deform and maintain a good seal. Although not shown on the schematic, a glass electrode pH sensor and an LM35 temperature sensor connected to data acquisition hardware were placed in the middle compartment. The reactor was primed by filling the middle compartment with water and the electrode compartments with 1 M KOH to allow the membranes to swell and to exchange counter-ions.

Equipment

The following commercial equipment was used: one SP10T pH/T combined sensor (Consort, Belgium), one LM35 semiconductor-based temperature sensor, two Reglo Digital MS-2/8 peristaltic pumps called PP1 and PP2 (ISMATECH, Switzerland), one Reglo Analog MS-2/8 peristaltic pump called PP3 (ISMATECH, Switzerland), one NI PCI-6259M data acquisition board (National Instruments, USA) inside of a pre-built computer, one analogical tachy-processor (Radiometer Analytical, France), one DXC236 potentiostat/galvanostat (P/G-stat) (Datronix Computers, Romania). For spectrometric measurements, one USB-4000 modular UV-VIS diode array spectrophotometer, two QP600-025-SR UV optical fibers, a FIA-Z-SMA-PEEK flow spectrophotometric cell with 10 mm optical path, a UV-VIS-NIR DT-MINI-2-GS light source, all from Ocean Optics (USA) were used. The AEM and CEM used in the reactor are a FUMASEP FAB-PK-130 (FUMATECH BWT GmbH, Germany) and a Nafion 423 (DuPont, France) respectively. Several pieces of proprietary equipment and software developed by Author S.-A. Dorneanu were also used.

Experimental setup

A simplified scheme of the experimental setup used during the diffusion and manual pH-stat tests is presented in Figure 10. The main elements are the FPER, the optical setup, the data acquisition and signal generation equipment and the pumps vehiculating liquids inside their circuits.

The catholyte and anolyte tanks (TC and TA) contained the 1 M or 0.1 M KOH solutions pumped in the electrode compartments. The THA tank contains the HBr + KBr + ARS solution which was injected into the

middle compartment and all collected liquid which reached the overflow was directed in the waste tank (TW). The pH and temperature sensors were connected via a proprietary equipment to the data acquisition system.

The FPER electrodes were connected to the working electrode (WE) and the counter electrode (CE) terminals of the P/G-stat, respectively. Silver wires, serving as reference electrodes, were introduced in the inlets of the electrode compartment and were connected to the REF1 and REF2 terminals of the P/G-stat. Initial experimental setup did not have the Mixer element, instead a teflon magnetic rod was used for stirring using the magnetic stirrer below. Later, the magnetic rod was removed and replaced by the Mixer pictured below, which was connected to the tachy-processor, for which the speed was set manually.

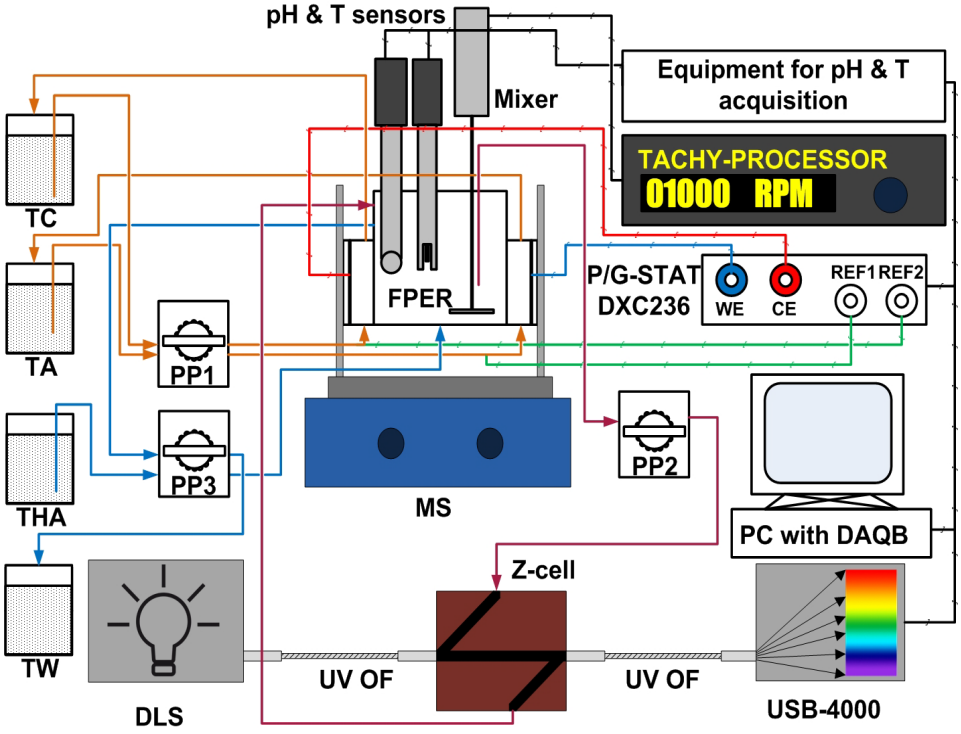

Figure 10. Experimental setup used for the diffusion and manual pH-stat tests: TC – Catholyte Tank; TA – Anolyte Tank; THA – HBr + ARS tank; TW – Waste Tank; PP – Peristaltic pump; MS – Magnetic Stirrer; DLS – Deuterium-Tungsten light source; UV OF – Ultra-violet optical fiber; FPER – filter press electrochemical reactor; P/G-STAT – potentiostat/galvanostat; PC with DAQB – PC with data acquisition board.

Though not shown on the schematic, the pumps, magnetic stirrer (and later tachogenerator) and light source were controlled by the computer through user input. Pump PP1 vehiculated the KOH solutions through the electrode compartments and pump PP2 completed the liquid circuit of the optical setup. Pump PP3 had a calibrated 1.5 mL/min tube which was used for acid addition and another tube of higher flow rate (20 mL/min) evacuating liquid from the overflow. For the initial standard addition tests of acid into ARS, PP1 was disconnected and the FPER was replaced with a simple mixing cell.

At the start of all FPER experiments, 36 mL of KBr 2 M and 0.7 mL of ARS 0.0125 M are added to the middle compartment of the reactor. TC and TA are filled with KOH solution and PP1 is run continuously over the course of the experiments. The HBr + KBr solutions used for addition were prepared in a 50 mL volumetric flask by adding appropriate volumes of stock KBr and HBr solutions and 1 mL of ARS 0.0125 M, resulting in approximately equal ARS concentrations for both addition and FPER solutions, thus avoiding the influence of indicator dilution. For diffusion tests, acid is added using PP2 until the desired pH is reached, after which it's stopped, and pH is monitored under no polarization. For pH-stat tests, pump PP2 is run continuously, and different currents are imposed by the P/G-stat through computer command. Current is manually adjusted until pH values stabilize.

Because of the complex behavior of proton activity and glass electrodes in high ionic strength solutions, we need to corroborate observed pH values using another method which functions on separate principles. Consequently, ARS was used as a witness pH indicator to validate pH values obtained by the glass electrode.

ACKNOWLEDGEMENTS

Author Gabriele-Mario Bogdan is grateful to Babeș-Bolyai University for the Special Scholarship for Scientific Activity (2024-2025), contract number 35809/28.11.2024.

REFERENCES

1. H. Marc; *La vie et les oeuvres de maitre Arnaud de Villeneuve*, Chamuel, Paris, **1896**.
2. G. Gauglitz; *Anal. Bioanal. Chem.*, **2018**, *410*, 1–3.
3. M. S. Kamble; M. S. S. Chougule; *IJARSCT*, **2022**, *2*.
4. D. J. Graham; B. Jaselskis; C. E. Moore; *J. Chem. Educ.*, **2013**, *90*, 345–351.

5. F. G. K. Baucke; *Fresenius' J. Anal. Chem.*, **1994**, *349*, 582–596.
6. L. Martell-Bonet; R. H. Byrne; *Mar. Chem.*, **2020**, *220*, 103764.
7. G. M. Silva; X. Liang; G. M. Kontogeorgis; *Mol. Phys.*, **2022**, *120*, e2064353.
8. M. N. Khan; P. Warrier; C. J. Peters; C. A. Koh; *J. Nat. Gas Sci. Eng.*, **2016**, *35*, 1355–1361.
9. L. Sun; Q. Lei; B. Peng; G. M. Kontogeorgis; X. Liang; *Fluid Phase Equilib.*, **2022**, *556*, 113398.
10. B. Anes; R. J. N. Bettencourt Da Silva; H. F. P. Martins; C. S. Oliveira; M. F. Camões; *Accred. Qual. Assur.*, **2016**, *21*, 1–7.
11. C. Fenster; M. Rohwerder; A. W. Hassel; *Mater. Corros.*, **2009**, *60*, 855–858.
12. R. E. Adams; S. R. Betso; P. W. Carr; *Anal. Chem.*, **1976**, *48*, 1989–1996.
13. F. A. Posey; T. Morozumi; E. J. Kelly; *J. Electrochem. Soc.*, **1963**, *110*, 1183.
14. A. D. Kalafatis; L. Wang; W. R. Cluett; *IFAC Proc. Vol.*, **2004**, *37*, 823–828.
15. S. Lee; S. W. Sung; J. Lee; *Int. J. Control Autom. Syst.*, **2013**, *11*, 442–449.
16. C. A. Pérez-Rojas; C. A. Martínez-Martínez; E. Palacios-Mechetnov; M. C. Lora-Vilchis; *Aquac. Eng.*, **2022**, *99*, 102300.
17. M. C. Palancar; J. M. Aragón; J. S. Torrecilla; *Ind. Eng. Chem. Res.*, **1998**, *37*, 2729–2740.
18. M. R. Pishvaie; M. Shahrokhi; *Ind. Eng. Chem. Res.*, **2000**, *39*, 1311–1319.
19. S. W. Sung; I.-B. Lee; D. R. Yang; *Ind. Eng. Chem. Res.*, **1995**, *34*, 2418–2426.
20. G.-M. Bogdan; M. I. Frîncu; S.-A. Dorneanu; *Studia UBB Chemia*, **2024**, *69*, 177–191.
21. G. Senanayake; *Miner. Eng.*, **2007**, *20*, 634–645.
22. A. Inagawa; A. Sasaki; N. Uehara; *Talanta*, **2020**, *216*, 120952.
23. A. A. Shalaby; A. A. Mohamed; *RSC Adv.*, **2020**, *10*, 11311–11316.
24. D. Asante-Sackey; S. Rathilal; E. Kweinor Tetteh; E. O. Ezugbe; L. V. Pillay; *Membranes*, **2021**, *11*, 358.
25. H. Fan; N. Y. Yip; *ACS EST Eng.*, **2022**, *2*, 2076–2085.
26. S. Ozkul; J. J. Van Daal; N. J. M. Kuipers; R. J. M. Bisselink; H. Bruning; J. E. Dykstra; H. H. M. Rijnaarts; *J. Membr. Sci.*, **2023**, *665*, 121114.
27. M. Tedesco; H. V. M. Hamelers; P. M. Biesheuvel; *J. Membr. Sci.*, **2016**, *510*, 370–381.
28. M. Tedesco; H. V. M. Hamelers; P. M. Biesheuvel; *J. Membr. Sci.*, **2017**, *531*, 172–182.